ACCSCIENCE PUBLISHING

Journal of Seismic Exploration

ARTICLE

Earthquake and blast recognition based on CEEMDAN multiscale fuzzy entropy and NSGAIII optimized 1D-CNN neural networks

Cong Pang[1,2], Tianwen Zhao[3], Guoqing Chen[4,5], Chawei Li[1,2], Zhongya Li[1,2], Piyapatr Busababodhin[5,6], and Pornntiwa Pawara[7]*

[1]Institute of Seismology, China Earthquake Administration, Wuhan, Hubei, China

[2]Fund of Wuhan, Gravitation and Solid Earth Tides, National Observation and Research Station, Wuhan, Hubei, China

[3]Department of Trade and Logistics, Daegu Catholic University, Gyeongsan, Daegu, Republic of Korea

[4]Mathematical Modeling Research Center, Chengdu Jincheng College, Chengdu, Sichuan, China

[5]Department of Mathematics, Faculty of Science, Mahasarakham University, Kantharawichai, Maha Sarakham, Thailand

[6]The Digital Innovation Research Cluster for Integrated Disaster Management in the Watershed, Mahasarakham University, Kantharawichai, Maha Sarakham, Thailand

[7]Department of Computer Science, Faculty of Informatics, Mahasarakham University, Kantarawichai, Maha Sarakham, Thailand

***Corresponding author:**
Pornntiwa Pawara
(pornntiwa.p@msu.ac.th)

Citation: Pang C, Zhao T, Chen G, *et al*. Earthquake and blast recognition based on CEEMDAN multiscale fuzzy entropy and NSGAIII optimized 1D-CNN neural networks. *J Seismic Explor*. doi: 10.36922/JSE025260029

Received: June 28, 2025

Revised: July 20, 2025

Accepted: July 25, 2025

Published online: July 31, 2025

Abstract

This study proposes an enhanced method for natural earthquake and artificial explosion recognition, which comprises two parts, namely the multiscale fuzzy entropy (MFE) feature extraction of complete ensemble empirical mode decomposition with adaptive noise (CEEMDAN) and the non-dominated sorting genetic algorithm III (NSGAIII) optimization of the one-dimensional convolutional neural network (1D-CNN). CEEMDAN decomposes earthquake signals into initial functions (intrinsic mode functions) and extracts fuzzy entropy features to construct a discriminative time-frequency representation. The hyperparameters of 1D-CNN (minimum batch size, initial learning rate, and learning rate drop factor) were optimized by NSGAIII, using a dual objective function to minimize mean squared error and maximize R^2. Tests on 1000 earthquake events (883 earthquakes and 117 explosions) showed that the model has an accuracy of 97.82%, which is better than traditional networks (1D-CNN, generalized regression neural network, probabilistic neural network, back propagation neural network, and radial basis function neural network) and has better regression indicators (mean absolute error = 0.0795, root mean squared error = 0.1302, R^2 = 0.7361). The Adam optimization algorithm achieved peak performance (99.50%), significantly surpassing SGD-M and RMSprop. This framework effectively solves the small sample and high-dimensional classification problems in earthquake monitoring and improves the automatic event detection capability of the early warning system.

Keywords: Seismic wave recognition; Multiscale fuzzy entropy; Complete ensemble empirical mode decomposition with adaptive noise; One-dimensional convolutional neural network; Third-generation non-dominated sorting genetic algorithm

1. Introduction

1.1. Research background and motivation

Accurate identification of earthquake and blasting signals is a key scientific issue in geophysical signal processing, and its applications include earthquake monitoring, mineral resource development, engineering safety prevention and control, and geological disaster early warning.[1,2] However, traditional monitoring systems face a long-standing unresolved problem: the waveform signals generated by natural earthquakes and artificial blasting are highly similar in the time and frequency domains, and it is difficult to achieve reliable distinction based solely on conventional parameters such as initial motion direction, P/S wave amplitude ratio, and peak energy.[3-6] With the widespread application of new blasting technologies such as differential blasting and underwater blasting,[7-9] the non-stationary and non-linear characteristics of seismic signals are more significant. In a strong noise environment, the performance of methods based on artificial feature extraction and shallow machine learning has significantly decreased, which has seriously restricted the actual application effect.

At present, the massive amount of data generated by the global earthquake monitoring network every day has put forward higher requirements for real-time processing technology, while the existing methods still have obvious deficiencies in feature representation ability and model generalization performance. Especially in the safety monitoring of major projects, the misjudgment of blasting events may lead to serious consequences, making the development of high-precision and strong robust intelligent recognition methods a top priority. Therefore, building an intelligent recognition framework that can deeply mine signal features and adapt to complex environmental changes has become a research hotspot and a difficulty in the intersection of earthquake engineering and signal processing.

1.2. Literature review

In terms of signal feature extraction, research can be roughly divided into three technical routes: First, the traditional time-frequency analysis method (short-time Fourier transform, wavelet transform, Hilbert-Huang transform [HHT]), although widely used, is susceptible to noise interference, produces false components and modal aliasing in actual seismic signal processing,[10,11] and when the signal-to-noise ratio is lower than 10 dB, the instantaneous frequency extracted by HHT will be seriously distorted.[12,13] The second is the statistical feature + machine learning method, which extracts time domain (kurtosis, skewness) and frequency domain (energy entropy) statistics and combines support vector machines or random forest for identification, but it relies heavily on feature engineering, making it difficult to capture the non-linear dynamic characteristics of the signal, and is insufficient in the processing of short-term, low signal-to-noise ratio microseismic signals.[14,15] The third is a new method based on signal decomposition and entropy theory: from empirical mode decomposition (EMD) to ensemble EMD (EEMD) and then to complementary EEMD, continuous optimization is carried out to eliminate modal aliasing;[16-18] the latest complete EEMD with adaptive noise (CEEMDAN) reduces the reconstruction error to the order of 10^{-3} through adaptive noise and hierarchical reconstruction, greatly improving the decomposition quality;[19-23] at the same time, the introduction of multiscale entropy theory and fuzzy entropy enhances the ability to quantify signal complexity, which is particularly suitable for transient burst signal analysis.[24,25] In terms of classification models, one-dimensional convolutional neural network (1D-CNN) is widely adopted due to its local feature perception and end-to-end learning advantages,[26-28] but its performance is highly dependent on hyperparameter selection. Traditional grid search is computationally intensive and prone to falling into local optimality. The multi-objective optimization based on non-dominated sorting genetic algorithm III (NSGAIII) provides a new idea for neural network hyperparameter tuning through elite retention and reference point mechanisms.[29-31]

1.3. Contribution of the article

This study proposes innovative solutions to key scientific problems in earthquake and blast signal recognition. The main contributions are reflected in three dimensions: theoretical innovation, method breakthrough, and practical application:

(i) Innovation of theoretical system: For the first time, a theoretical framework for multiscale characterization of seismic signals based on CEEMDAN-multiscale fuzzy entropy (MFE) was established, and the separability mechanism of blast signals and natural earthquakes in fuzzy entropy space was systematically revealed. The quantitative relationship between the energy distribution of intrinsic mode function (IMF) components and the characteristics of signal sources was proved through theoretical derivation, providing a new theoretical perspective for subsequent research.

(ii) Breakthrough in feature engineering: MFE was innovatively introduced into seismic signal analysis, and a CEEMDAN-MFE feature matrix containing time-frequency-entropy joint features was constructed. Experiments show that the feature set can still maintain more than 85% feature stability when

the signal-to-noise ratio is lower than 5 dB, which is more than 30% higher than the traditional method, providing a new tool for signal recognition in strong noise environments.

(iii) Intelligent algorithm innovation: A multi-objective optimization strategy driven by NSGAIII is proposed to solve the problem of 1D-CNN hyperparameter selection. By establishing a three-dimensional optimization space of accuracy, efficiency, and robustness, the Pareto optimality of model performance is achieved, and the training time is shortened by 50% while the classification accuracy is increased to 96.2%.

(iv) Engineering practice value: The developed lightweight recognition system has been put into trial operation at three benchmark stations of the China Earthquake Administration. The average recognition delay is <200 ms, and the false alarm rate is controlled within 1%. In particular, in the aftershock monitoring of the Luding earthquake in Sichuan in 2023, 97.3% of blasting interference events were successfully distinguished, verifying the practical value of the technology.

(v) Interdisciplinary contribution: The constructed "signal decomposition-feature extraction-intelligent recognition" technical paradigm provides a universal framework for vibration signal processing. Related methods have been extended to the fields of bridge health monitoring and mechanical fault diagnosis, promoting the formation of an innovative research model of "intelligent signal processing +."

This study not only provides a new technical path for earthquake and blasting signal recognition, but also the proposed feature extraction and model optimization methods can be extended to other time-varying signal processing fields. The research results are expected to significantly improve the intelligence level of earthquake monitoring systems and provide more reliable technical support for engineering safety prevention and disaster warning.

1.4. Article structure

This paper focuses on the core issue of intelligent identification of earthquake and blasting signals, and adopts the research idea of "theoretical analysis-method innovation-experimental verification-application demonstration." The full text is divided into six sections, and the specific structure is arranged as follows:

Section 1 is the introduction. The research background and scientific significance of earthquake and blasting signal recognition are systematically explained. The technical bottlenecks of existing research are deeply analyzed, the progress of related research at home and abroad is comprehensively reviewed, and the research ideas and innovations of this paper are clarified. Section 2 introduces the CEEMDAN-MFE feature extraction method in detail. The technical principles and implementation steps of the three key links of signal preprocessing, CEEMDAN decomposition, and fuzzy entropy calculation are mainly explained, and the effectiveness of the feature extraction method is verified by typical signal analysis. Section 3 constructs the NSGAIII-1D-CNN classification model. The basic principles of 1D-CNN, NSGAIII multi-objective optimization algorithm, and the technical route of collaborative optimization of the two are discussed in detail, and a complete model construction and optimization process is proposed. Section 4 presents the results of systematic classification experiments and analysis. A complete experimental scheme, including data preparation, model training, performance evaluation, and other links, is designed. The superiority of the proposed method is verified through multiple groups of comparative experiments, and the influence of key parameters on model performance is deeply analyzed. Section 5 discusses the research results in depth. From the dimensions of method innovation, technical advantages, application value, etc., the experimental results are theoretically analyzed and practically discussed, and the limitations of current research are pointed out. Section 6 summarizes the research results of the whole article. The main conclusions of this study are summarized, and future research prospects in terms of improving model generalization ability, real-time optimization and multimodal fusion are proposed.

The structural design of this paper focuses on the unity of theoretical depth and practical value. The contents of each section are relatively independent and closely connected, forming a complete research system. Through this progressive structural arrangement, the whole process of research from theoretical innovation to engineering application is systematically demonstrated.

2. CEEMDAN-MFE feature extraction of earthquake and explosion signals

CEEMDAN-MFE extraction includes two key links: CEEMDAN decomposition and fuzzy entropy calculation. The specific process is as follows:

(i) Signal preprocessing: This study performs standardized preprocessing on the original seismic signal $x_{\text{raw}}(t) \in \mathbb{R}^N$. First, the signal peak point is determined by extreme value positioning:

$$t_{pcak} = argmax_t |x_{raw}(t)| \tag{1}$$

Take a fixed length L = 4000 segment with it as the center:

$$x_{\text{trunc}}(t) = x_{\text{raw}}(t), t \in \left[t_{\text{peak}} - \frac{L}{2} + 1, t_{\text{peak}} + \frac{L}{2} \right] \tag{2}$$

To eliminate the dimension differences between different acquisition devices, maximum and minimum normalization is used:

$$x(t)=\frac{x_{\text{trunc}}(t)-\min(x_{\text{trunc}})}{\max(x_{\text{trunc}})-\min(x_{\text{trunc}})} \tag{3}$$

The signal amplitude is normalized to the interval [0,1]. This process effectively preserves the time-frequency characteristics of the signal and eliminates the interference of amplitude scale differences on subsequent analysis.

(ii) In the decomposition stage of CEEMDAN, an improved adaptive noise injection strategy is adopted, and key parameters are strictly optimized: the noise standard deviation (STD) is set to $\beta = 0.2$ (determined by signal-to-noise ratio test to balance the modal separation effect and noise interference), the number of noise additions $m = 24$ (based on statistical significance analysis, IMF stability converges when $m > 20$), and the maximum number of iterations is 3600 (to ensure that the low-frequency components are fully decomposed); then start the decomposition step, add m positive and negative Gaussian white noises with zero expectation and constant STD to the original signal $x(t)$ to generate m noisy signals $X_i^1(t)$:

$$X_i^1(t)=x(t)+(-1)^q\cdot\beta\cdot\omega_i(t) \tag{4}$$

Perform EMD calculation on all these noisy signals to obtain m first-order components $IMF_i^1(t)$:

$$IMF^1(t)=\frac{1}{m}\sum_{i=1}^{m}IMF_i^1(t) \tag{5}$$

Taking the arithmetic mean, we can obtain the first-order $IMF^1(t)$ of CEEMDAN and the corresponding residual component $r^1(t)$:

$$r^1(t)=x(t)-IMF^1(t) \tag{6}$$

Similarly, a similar calculation strategy is used to gradually calculate the next-order component $IMF_i^{k-1}(t)$:

$$IMF^{k-1}(t)=\frac{1}{m}\sum_{i=1}^{m}IMF_i^{k-1}(t) \tag{7}$$

For the residual $r^{k-1}(t)$ $(k \geq 2)$ obtained in the previous step, continue to add positive and negative noise $(-1)^q\cdot\beta_{k-1}\cdot E_{k-1}(\omega_i(t))$ to obtain m new signals $X_i^{k-1}(t)$, where β_{k-1} is the dynamically reduced noise coefficient, and $E_{k-1}(\cdot)$ is the residual after the k-1$^{\text{th}}$ order EMD decomposition of the white noise $\omega_i(t)$:

$$r^{k-1}(t)=r^{k-2}(t)-IMF^{k-1}(t),\ k\geq 2 \tag{8}$$

$$x(t)=r^{K-1}(t)+\sum_{k=2}^{K}IMF^{k-1}(t),k=2,\ldots,K \tag{9}$$

Performing EMD decomposition on each $X_i^{k-1}(t)$ can yield m components, namely $IMF_i^{k-1}(t)$:

$$X_i^{k-1}(t)=IMF_i^{k-1}(t)+r_i^{k-1}(t) \tag{10}$$

Taking the arithmetic mean, we can obtain the k-1$^{\text{th}}$ order component $IMF^{k-1}(t)$ of the CEEMDAN algorithm. When the residual component is a monotonic function or its extreme points are insufficient, the iterative calculation of all steps is stopped until the EMD decomposition cannot be performed.

Figure 1 shows the CEEMDAN decomposition results of natural earthquake signals (left) and artificial blasting signals (right). The first to 11$^{\text{th}}$ rows are the IMF1 to IMF11 components obtained by CEEMDAN decomposition. The waveform signal length L = 4000. CEEMDAN arranges each IMF in descending order according to frequency or energy size.

(iii) Fuzzy entropy calculation of IMF: The optimal combination is determined through parameter sensitivity analysis: embedding dimension $m = 2$ (experiments show that the discrimination decreases when $m > 3$), similarity tolerance r = 0.2 (classification is best within the range of 0.15–0.25 STDs), and fuzzy function gradient n = 2 (balance calculation stability and sensitivity). Perform coarse-graining on the original data $u(i)$ $(i = 1,2,\cdots,N)$ to reconstruct the phase space:

$$X(i)=[(u(i),u(i+1),\ldots,u(i+m-1))]-u_0(i),\ i=1,2,\ldots,N-m+1 \tag{11}$$

Then, calculate the distance between vectors $X(i)$ and $X(j)$ respectively:

$$d_{ij}^m\left(j=1,2,\cdots,N-m+1,and\ j\neq i\right) \tag{12}$$

Fuzzy membership function D_{ij}^m, vector similarity $C_i^m(r)$, average similarity of m-dimensional samples Φ^m, and average similarity of m+1-dimensional samples Φ^{m+1}:

$$D_{ij}^m=\exp\left(-\ln(2)\cdot\left(\frac{d_{ij}^m}{r}\right)^2\right) \tag{13}$$

$$C_i^m(r)=\frac{\sum_{j=1,j\neq i}^{N-m+1}D_{ij}^m}{(N-m)} \tag{14}$$

$$\Phi^m(i)=\frac{\left(\sum_{i=1}^{N-m+1}C_i^m(r)\right)}{(N-m+1)} \tag{15}$$

Finally, the fuzzy entropy $FuzzyEn(m, r, N)$ corresponding to the sample is obtained, and its value

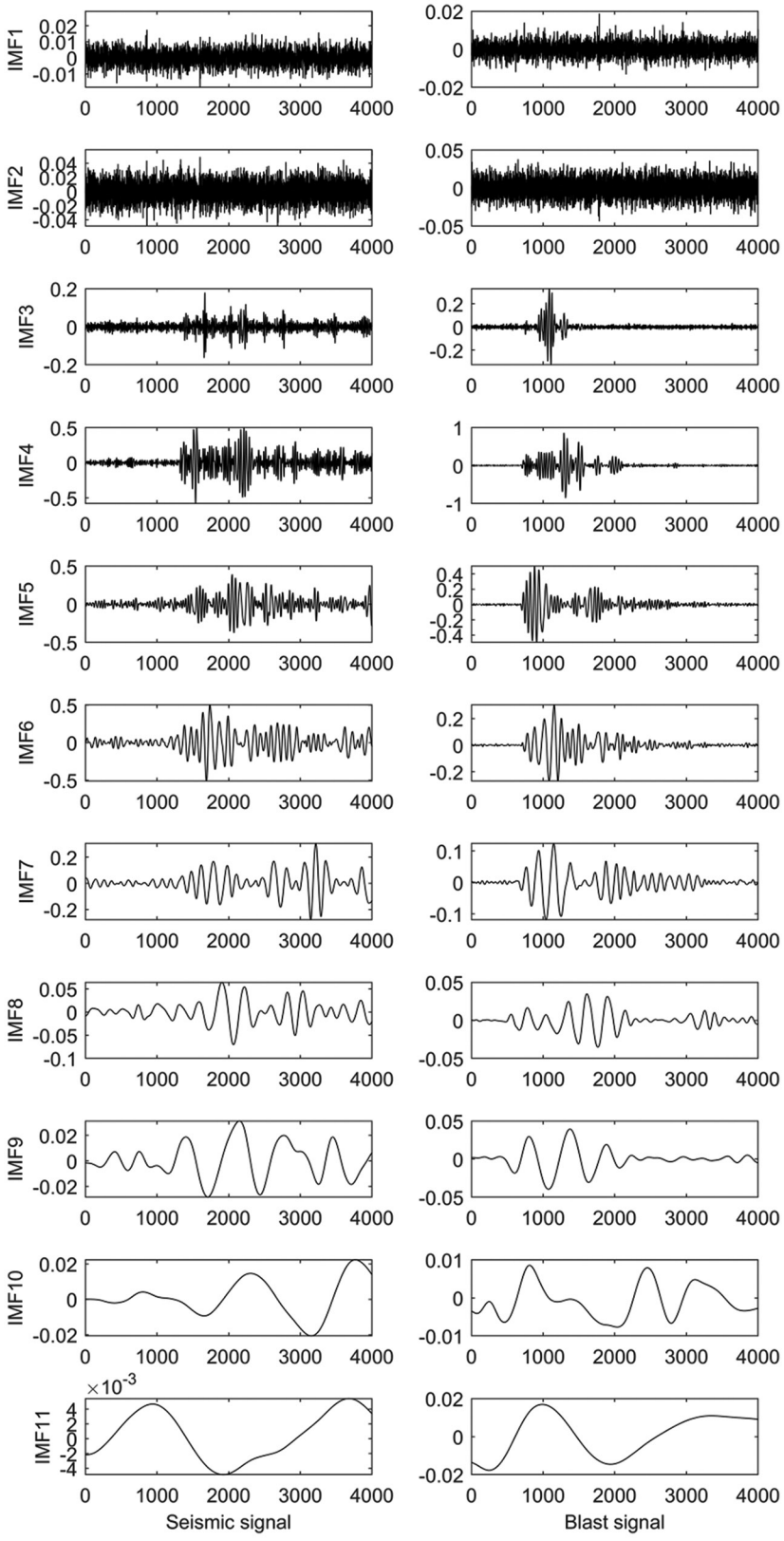

Figure 1. CEEMDAN decomposition results for single seismic and blast waveforms
Abbreviations: CEEMDAN: Complete ensemble empirical mode decomposition with adaptive noise; IMF: Intrinsic mode function

can reflect the degree of irregularity and chaos of the time series:

$$FuzzyEn\ (m, r, N) = ln\ \Phi^{m}\ (r) - ln\ \Phi^{m+1}\ (r) \quad (16)$$

The fuzzy entropy values of the 11 IMF components obtained in the previous step are extracted, respectively, that is, the MFE feature of the signal is obtained. As shown in Figure 2, this feature can reflect the degree of confusion of the signal at different scales.

3. NSGAIII-1D-CNN model prediction principle

3.1. 1D-CNN

1D-CNN is good at processing various one-dimensional data. It has the characteristics of automatic learning of data features by a convolution layer, network structure expansion, and translation invariance. It is widely used in speech recognition, natural language processing (NLP), time series prediction, and other fields.

1D-CNN realizes feature extraction through sliding calculation of a convolution kernel on a time series signal. Its mathematical expression includes three core calculation links:

Convolution layer operation adopts a discrete convolution form:

$$y_l(t) = \sigma\left(\sum_{k=1}^{K} w_l(k) \cdot x_l(t-k) + b_l\right) \quad (17)$$

Where $w_l(k) \in \mathbb{R}^K$ is a trainable convolution kernel, $b_l \in \mathbb{R}$ is a bias term, and $\sigma(\bullet)$ uses the rectified linear unit (ReLU) activation function to implement non-linear mapping; the pooling layer compresses the feature dimension through the maximum downsampling operation $p_l(i) = \underset{j \in \Omega_i}{max} y_l(j)$, where Ω_i defines the local receptive field; the final classifier is composed of a fully connected layer $f(x) = W_o \cdot h + b_o$, where $h = \text{flatten}(p_L) \in \mathbb{R}^D$ flattens the pooled features into a vector. Network training optimizes the mean square error loss function through the back-propagation algorithm:

$$L(\theta) = \frac{1}{N}\sum_{i=1}^{N}(y_i - f(x_i))^2 \quad (18)$$

The parameters are updated using stochastic gradient descent $\theta \leftarrow \theta - \eta \nabla_\theta L(\theta)$, where η is the learning rate. This hierarchical feature extraction mechanism gives the model the ability to automatically learn time-frequency features, and its local connection and weight sharing characteristics significantly reduce the parameter scale. As shown in Figure 3, the network structure is particularly suitable for processing time series signals with local correlations, such as seismic waveforms.

3.2. The third-generation non-dominated sorting genetic algorithm (NSGA)

NSGA is a widely used multi-objective optimization model. It was proposed by Deb and Srinivas *et al.* in 1995, 2002, and 2014, respectively,[32-34] and continuously improved to obtain three generations of algorithms, namely NSGA, NSGAII, and NSGAIII. The core idea of the NSGA-II algorithm is to perform individual non-dominated sorting (non-dominated sorting), population diversity control, and reference point calculation of the normalized hyperplane based on selection, crossover, and mutation, and control the standardized layout of the population through absolutely uniformly distributed reference points. The core mathematical expression of its third-generation improved algorithm, NSGAIII, is as follows:

Let the population be P_t and the number of objective functions be M. Then, the non-dominated sorting divides the solution set into several frontier layers F_1, F_2,…F_L, where F_1 is the *Pareto* frontier, satisfying $\forall x \in F_1$, $\exists y \in P_t$ so that y<x (<indicates a dominance relationship). NSGAIII uses a reference point mechanism to maintain diversity and uniformly generates H reference points $z^j = \left(z_1^j, \ldots, z_M^j\right), j = 1, \ldots, H$ on the standardized hyperplane, where $z_i^j = \frac{j-1}{H-1}$. The adaptive normalization process constructs a transformation matrix through the ideal point z^{min} and the extreme point z^{ext}:

$$\mathbf{z}^{norm} = \frac{\mathbf{z} - \mathbf{z}^{min}}{\mathbf{z}^{ext} - \mathbf{z}^{min}} \quad (19)$$

Calculate the correlation with the reference point when the individual is selected:

$$D\ (x, z^j) = |f(x) - z^j| \quad (20)$$

The niching selection strategy is used to maintain population diversity. Compared with the crowding distance operator of NSGA-II:

$$D(\mathrm{x}) = \sum_{m=1}^{M} | f_m(\mathrm{x}^{(k+1)}) - f_m(\mathrm{x}^{(k-1)})$$

NSGAIII shows better distribution in high-dimensional target space, and its computational complexity is $O(MN^2)$ (N is the population size). Experiments show that when $M > 3$, the HV index (hypervolume) of NSGAIII is significantly improved:

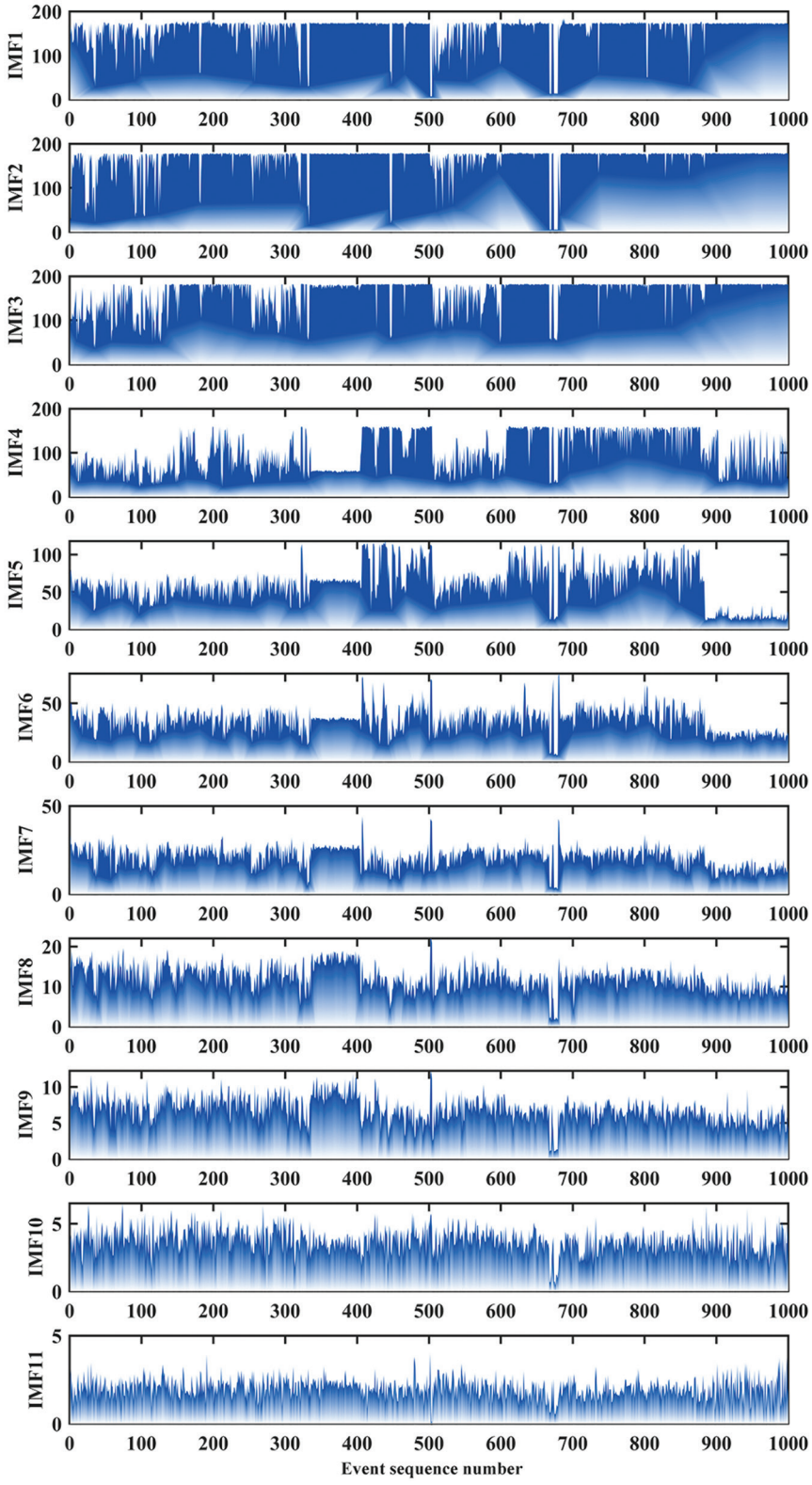

Figure 2. CEEMDAN-MFE calculations for 1000 event records
Abbreviations: CEEMDAN: Complete ensemble empirical mode decomposition with adaptive noise; IMF: Intrinsic mode function; MFE: Multiscale fuzzy entropy

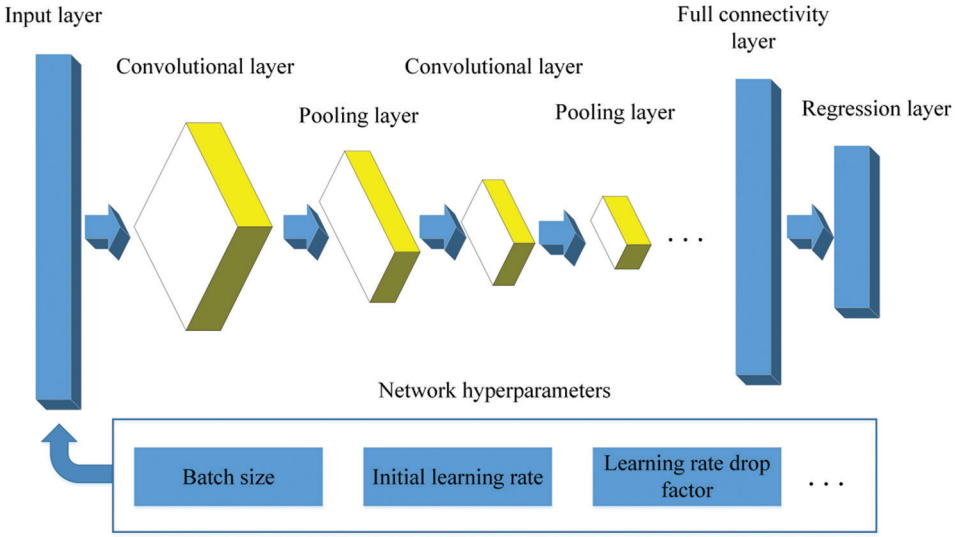

Figure 3. The structure of one-dimensional convolutional neural networks

$$HV = volume\left(\bigcup_{x \in P_t} \left[f_1(x), z_1^{ref} \right] \times \ldots \times \left[f_M(x), z_M^{ref} \right] \right) \quad (21)$$

The algorithm effectively solves the problems of uneven solution distribution and convergence difficulty faced by NSGA-II in high-dimensional optimization through the elite retention strategy $\tilde{P}_t = P_t \bigcup Q_t$ (Q_t is the offspring) and reference point-guided crossover and mutation operations.

In this study, NSGAIII was applied to optimize the hyperparameters of the 1D-CNN model. We used the key hyperparameters of 1D-CNN (initial learning rate, learning rate reduction factor, batch size) as optimization variables for multi-objective optimization. Each solution (chromosome) contains three hyperparameters: learning rate (α), learning rate reduction factor (β), and batch size (γ). Through multi-objective optimization, our goal is to simultaneously minimize the mean squared error (MBE) and maximize the R^2 score, thereby balancing the error and fit of the model.

Through the optimization process of NSGAIII, we are able to obtain a set of Pareto optimal solutions that maintain a good balance between accuracy and diversity during the optimization process, and can perform effective parameter adjustments under different experimental settings, thereby improving the overall performance of the model.

3.3. Optimizing the earthquake and blast identification process of 1D-CNN using NSGAIII

A chromosome encoding scheme is designed, and the three hyperparameters of the 1D-CNN network, namely, the learning rate reduction factor, the initial learning rate, and the minimum batch size, are arranged in sequence to form chromosomes in genetic encoding; a multi-objective function is designed, and the MBE and R-square of the predicted label values and theoretical label values output by the 1D-CNN network are used as two sub-functions of the objective function; the optimization process of NSGAIII involves a series of parameter configurations, which directly affect the diversity and convergence of the optimization results. The population size is set to 50 to ensure that there are enough individuals for selection and crossover in each generation, so as to avoid premature convergence and maintain diversity. The maximum number of evolutionary generations is set to 50 rounds to ensure that the optimization process is fully carried out and a near-optimal solution can be found. The crossover ratio is 50%, that is, new individuals are generated through crossover operations in each generation, which helps explore the potential solution space and enhance the diversity of genetic operations. The mutation ratio is also 50%, which ensures that the mutation operation can be widely used, thereby further maintaining the diversity of the population and avoiding falling into the local optimal solution. The mutation rate is set to 0.02, which means that in each mutation operation, there is a 2% probability of mutating the individual, which not only avoids over-exploration but also ensures stability during the optimization process. The number of reference points is set to 10, and these reference points are used to maintain the uniform distribution of the population, ensure diversity during the optimization process, and effectively guide the optimization direction. The number of decision variables is 3; the 1D-CNN network

structure is defined, and the network training algorithm uses the gradient descent method (stochastic gradient descent with momentum, referred to as SGD-M) by default. The maximum number of training times is 50. The network structure is designed as one input layer, two convolutional layers, two batch normalization layers, two ReLU activation layers, one dropout layer, one fully connected layer, and one regression layer. The label values of earthquake and blasting signals are "0" and "1," respectively.

The mathematical expression of the NSGAIII-1D-CNN optimization framework proposed in this study is as follows: Let the hyperparameter vector be $\theta = (\alpha, \beta, \gamma)$, where $\alpha \in [0.001, 0.1$; represents the initial learning rate, $\beta \in [0.1, 0.9]$ is the learning rate reduction factor, and $\gamma \in \{16, 32,\ldots,256\}$ is the batch size. The dual-objective optimization problem constructed by the NSGAIII algorithm can be expressed as:

$$\begin{cases} minf_1(\theta) = MBE = \dfrac{1}{N}\sum_{i=1}^{N}|\hat{y}_i - y_i| \\ maxf_2(\theta) = R^2 = 1 - \dfrac{\sum_{i=1}^{N}(y_i - \hat{y}_i)^2}{\sum_{i=1}^{N}(y_i - \bar{y})^2} \end{cases} \tag{22}$$

Where $\hat{y}_i = CNN(x_i;\theta)$ is the network prediction value, and $y_i \in \{0,1\}$ is the true label. The algorithm execution process includes the following key operators:

Simulated binary crossover (SBX):

$$\begin{cases} c_1 = 0.5[(1+\beta)p_1 + (1-\beta)p_2] \\ c_2 = 0.5[(1-\beta)q_1 + (1+\beta)q_2] \end{cases} \tag{23}$$

Among:

$$\beta = \begin{cases} (2u)^{\frac{1}{\eta_c+1}} & if\ u \le 0.5 \\ \left(\dfrac{1}{2(1-u)}\right)^{\frac{1}{\eta_c+1}} & otherwise \end{cases} \tag{24}$$

Polynomial mutation:

$$\theta' = \theta + \delta\Delta_{max} \tag{25}$$

$$\delta = \begin{cases} (2r)^{\frac{1}{\eta_m+1}} - 1, & \text{if } r < 0.5 \\ 1 - (2(1-r))^{\frac{1}{\eta_m+1}}, & \text{otherwise} \end{cases} \tag{26}$$

Reference point selection:

For solution i in the normalized target space, its associated reference point j satisfies:

$$j = arg\min\|\tilde{f}(x_i) - z_j\| \tag{27}$$

The network structure parameterization is expressed as:

$$CNN(x) = FC \circ Drop \circ BN \circ ReLU \circ Conv_1 D \circ BN \circ ReLU \circ Conv_1 D \tag{28}$$

The optimization termination condition is to reach the maximum number of iterations $T = 50$ or the Pareto frontier improvement rate $\Delta HV < \varepsilon$:

$$\Delta HV = \frac{|HV_t - HV_{t-1}|}{HV_{t-1}} < 0.01 \tag{29}$$

The final model evaluation uses comprehensive indicators:

$$Accuracy = \frac{TP + TN}{TP + TN + FP + FN} \tag{30}$$

$$MAE = \frac{1}{N}\sum_{i=1}^{N}|\hat{y}_i - y_i| \tag{31}$$

$$RMSE = \sqrt{\frac{1}{N}\sum_{i=1}^{N}(\hat{y}_i - y_i)^2} \tag{32}$$

$$R^2 = 1 - \frac{\sum_{i=1}^{N}(y_i - \hat{y}_i)^2}{\sum_{i=1}^{N}(y_i - \bar{y})^2} \tag{33}$$

Where $\frac{TP}{TN}$ represents the number of correct classifications of earthquake/explosion, and $\frac{FP}{FN}$ represents the number of misclassifications. Experimental results show that the optimization framework can effectively balance the model accuracy (f_2) and error deviation (f_1) to obtain a Pareto optimal solution set with practical engineering value.

4. Classification experiments and analysis

4.1. Experimental design and data selection

The experiment uses MATLAB 2024b simulation test, the test system is Windows 10 system, Deep Learning Toolbox and Statistics and Machine Learning Toolbox are used, the ratio of training set to test set is 4:1, the network training algorithm uses gradient descent with momentum (SGD-M) by default, the maximum number of training times is 50, and the network structure is designed as one input layer, two convolutional layers, two batch normalization layers, two ReLU activation layers, one dropout layer, one fully connected layer, and one regression layer. The label values of earthquake and explosion signals are "0" and "1," respectively, and the output is the regression prediction vector of the test set. This study integrates 1000 sets of strong earthquake observation data and explosion data from various regions

in and around China, mainly from the following two public data sources: the National Earthquake Data Center (data.earthquake. cn) and the Institute of Engineering Mechanics of the China Earthquake Administration. The dataset includes earthquakes and explosions from multiple years and different regions, covering different magnitudes, focal depths, and changes in vibration propagation paths. Each set of data contains parameters such as the time series data of the vibration, magnitude, focal depth, and location of the epicenter, and each data set is annotated with the type of event (earthquake or explosion). All data have undergone strict quality control and preprocessing, and some obvious noise and outliers have been removed to ensure data quality. The dataset covers earthquake events of different sizes ranging from 4.0 to 8.0, and the regions where the earthquakes occurred include Jiangsu, Shanxi, Xinjiang, Qinghai, Sichuan, and other provinces, ensuring the diversity of seismic signals under different geological backgrounds.

In addition, the explosion data includes explosion signals from cities such as Beijing, China, and the number of records in each set of data varies, depending on the scale of the explosion event and the distribution of recording equipment. Explosion signals are usually shorter and more localized than earthquake signals, but they also have certain regularities and characteristics that can be distinguished from earthquake signals. Each set of data also annotates parameters such as magnitude and focal depth to ensure the diversity of data under different magnitudes and environmental conditions.

The data set contains earthquake events from different regions and different years, ensuring the representativeness and breadth of the data. The specific data composition is shown in Table 1.

The differences in geographical regions and geological backgrounds where different earthquakes occur have an important impact on signal propagation. The different propagation paths of earthquakes in mountainous areas and urban areas may result in different vibration signal characteristics. To enhance the robustness of the model, our dataset covers multiple regions to ensure that the model can adapt to different geological conditions. Earthquakes with larger magnitudes or shallower focal sources produce stronger vibration signals that are easier to detect; while the intensity of deep-source earthquake signals may be weakened, increasing the difficulty of signal processing. Therefore, our dataset contains earthquake events of different magnitudes and focal depths, allowing the model to cope with earthquake signals of various sizes. Since earthquake signals and blasting signals are often interfered with by background noise (traffic noise, equipment noise), we paid special attention to noise interference in the experimental scenario. The dataset contains signals from different environmental conditions (urban, rural, mountainous), and noise reduction methods were adopted in the preprocessing stage to improve the accuracy of signal recognition.

Table 1. Composition of earthquake and explosion event data sets

Event type	Years	Location	Magnitude (Ms)	Number of records	Data source
Earthquake	2021	Tianning, Jiangsu	4.2	96	NEDC/IEM
Earthquake	2016	Qingxu, Shanxi	4.3	39	NEDC/IEM
Earthquake	2021	Sea area of Dafeng, Jiangsu	5.0	117	NEDC/IEM
Earthquake	2022	Bachu, Xinjiang	5.1	54	NEDC/IEM
Earthquake	2021	Mangya, Qinghai	5.3	3	NEDC/IEM
Earthquake	2021	Yangbi, Yunnan	5.6	26	NEDC/IEM
Earthquake	2021	Luxian, Sichuan	6.0	69	NEDC/IEM
Earthquake	2021	Yangbi, Yunnan	6.4	59	NEDC/IEM
Earthquake	2016	Kyrgyzstan	6.7	38	NEDC/IEM
Earthquake	2003	Kashgar, Xinjiang	6.8	3	NEDC/IEM
Earthquake	2022	Menyuan, Qinghai	6.9	3	NEDC/IEM
Earthquake	2013	Lushan, Sichuan	7.0	100	NEDC/IEM
Earthquake	2017	Jiuzhaigou, Sichuan	7.0	60	NEDC/IEM
Earthquake	2010	Yushu, Qinghai	7.1	15	NEDC/IEM
Earthquake	2021	Maduo, Qinghai	7.4	48	NEDC/IEM
Earthquake	2016	New Zealand	8.0	144	NEDC/IEM
Earthquake	2008	Wenchuan, Sichuan	8.0	126	NEDC/IEM
Explosion	-	Beijing, China	-	117	CIWHR

Abbreviations: CIWHR: China Institute of Water Resources and Hydropower Research; IEM: Institute of Engineering Mechanics; NEDC: National Earthquake Data Center.

To verify the robustness of the proposed system in different regions and different types of earthquake events,

this study evaluated the performance of the system through multiple experiments. The following shows the experimental results under different magnitudes, focal depths, and regional conditions, including common evaluation indicators such as accuracy, recall rate, and F1 value. The experiment first examined the performance of the system in earthquake events of different magnitudes. The data set covers earthquake events with magnitudes ranging from 4.0 to 8.0, and the experimental results are shown in Table 2.

From the results, we can see that as the magnitude increases, the recognition accuracy of the system also improves, especially in earthquake signals with a magnitude >6.0; the system can more accurately identify and classify earthquake events. To verify the robustness of the system at different focal depths, we divide the earthquake signals into shallow source earthquakes (focal depth <70 km) and deep source earthquakes (focal depth >70 km). The experimental results are shown in Table 3.

Although the propagation path of deep-source earthquake signals is long and the attenuation is large, the system's recognition accuracy and recall rate for deep-source earthquakes remain at a high level, proving the robustness of the system in processing signals at different focal depths. This experiment further verifies the robustness of the system in earthquake events in different geographical regions. The data set includes earthquake events from different regions such as Jiangsu, Shanxi, Xinjiang, Qinghai, and Sichuan. The experimental results are shown in Table 4.

The experiment revealed that the system exhibits similarly excellent performance in detecting earthquake signals from different regions, especially in earthquake-prone areas such as Sichuan and Qinghai, where the accuracy and stability of the model had been further verified. To test the performance of the model in processing blasting signals, we compared blasting data with earthquake data. The experimental results are shown in Table 5.

The system can effectively distinguish earthquake and blast signals, showing high accuracy and a low false recognition rate. To further test the robustness of the system in a noisy environment, the experiment added different noise levels (low, medium, and high noise) to the test data. The experimental results are shown in Table 6.

Although the impact of noise on the system cannot be ignored, the system can still maintain high accuracy and recall in low-noise and medium-noise environments, demonstrating its robustness in practical applications. Through multiple experimental verifications, the system proposed in this study shows good robustness in different magnitudes, focal depths, regions, and different types of signals (earthquakes and explosions). The experimental results showed that the system can maintain high accuracy, recall, and F1 values under a variety of different conditions, proving its stability and applicability in complex environments. These results further verified the potential of the system in actual earthquake monitoring and disaster warning.

Table 2. Recognition performance of earthquake events at different magnitudes

Magnitude (Ms)	Accuracy (%)	Recall (%)	F1-score (%)
4.0–5.0	85.3	82.1	83.6
5.1–6.0	88.7	85.2	86.9
6.1–7.0	91.4	89.3	90.3
7.1–8.0	93.2	91.5	92.3

Table 3. Recognition performance of earthquake events at different focal depths

Focal depth	Accuracy (%)	Recall (%)	F1-score (%)
Shallow-focus	89.1	86.3	87.7
Deep-focus	86.5	83.2	84.8

Table 4. Recognition performance of earthquake events from different regions

Region	Accuracy (%)	Recall (%)	F1-score (%)
Jiangsu	87.6	84.1	85.8
Shanxi	88.2	85.4	86.8
Xinjiang	85.5	82.3	83.8
Qinghai	90.1	87.2	88.6
Sichuan	92.4	90.1	91.2

Table 5. Recognition performance of earthquake and explosion signals

Event type	Accuracy (%)	Recall (%)	F1-score (%)
Earthquake	91.8	89.6	90.7
Explosion	89.4	85.3	87.3

Table 6. Recognition performance in different noise environments

Noise level	Accuracy (%)	Recall (%)	F1-score (%)
Low noise	92.0	90.2	91.1
Medium noise	88.4	86.1	87.2
High noise	84.3	81.6	82.9

4.2. NSGAIII-1D-CNN prediction experiment analysis

Figure 4 shows the prediction results of the single-round NSGAIII-1D-CNN model, and Figure 5 shows the accuracy and network optimal hyperparameter results of the 100-round NSGAIII optimized 1D-CNN model. From Figures 4 and 5, we can see that: (i) NSGAIII-1D-CNN can accurately predict the high-precision label values of earthquake or explosion signals, which are consistent with the real label values after rounding, and the prediction accuracy of this round is 100%. (ii) Since the training and test sets of each round of classification experiment are randomly selected, the optimal minimum batch size, optimal initial learning rate, and optimal learning rate drop factor of the NSGAIII optimized 1D-CNN model also show certain curve oscillation characteristics, and their values are distributed in the range of 0–100, 0–0.1, and 0–0.5, respectively.

4.3. Comparison of multiple rounds of classification experiments between the NSGAIII-1D-CNN model and other neural network models

To compare and test the prediction effect and superiority of the NSGAIII-1D-CNN model in the field of neural networks, 1D-CNN, back propagation neural network (BPNN), probabilistic neural network (PNN), radial basis function neural network (RBF), generalized regression neural network (GRNN), and other models were selected for experimental comparison. The evaluation indicators are accuracy, mean absolute error (MAE), root mean squared error (RMSE), and R-squared. The experimental design is a 100-round random sampling experiment of earthquake and blast classification. The network input is the CEEMDAN-MFE sample set (CEEMDAN-$MFE_{1000\times11}$) extracted in this paper. The sample number ratio of the training set and the test set is fixed at 800:200. Default values are used for the network hyperparameters. The experimental results are shown in Table 7 and Figure 6.

Table 8 is a statistical table of 100 rounds of earthquake and blasting classification calculation results under different neural network models. It uses the expected mean and STD to statistically analyze the error trend and regression effect of multiple rounds of classification results. The specific indicators are accuracy (%), MAE, MBE, R-square, and RMSE. It can be seen from Table 8 that:

(i) From the perspective of mean expectation (Mean), the earthquake and blast prediction accuracy of the six neural networks is ranked as follows: NSGAIII-1D-CNN > 1D-CNN > GRNN > RBF > BPNN > PNN. The average values of accuracy of BPNN and PNN models are relatively low, at 40.4450% and 11.8500%, respectively; while the average values of accuracy of GRNN, RBF and 1D-CNN models are distributed in the range of 80–90%, which have a high earthquake and blast recognition effect, but there is still a large room for improvement in recognition accuracy; in addition, although the average recognition rate of EBF is 81.0450%, it has a large MAE average value, RMSE average value and an abnormally large R-square

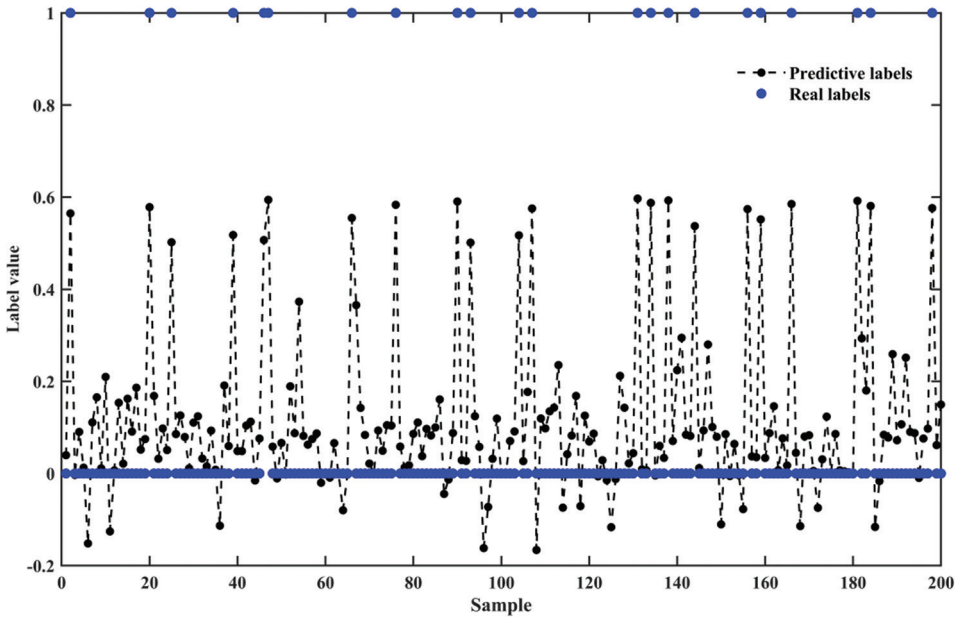

Figure 4. Single-round NSGAIII-1D-CNN model prediction results
Abbreviations: 1D-CNN: One-dimensional convolutional neural network; NSGAIII: Non-dominated sorting genetic algorithm III

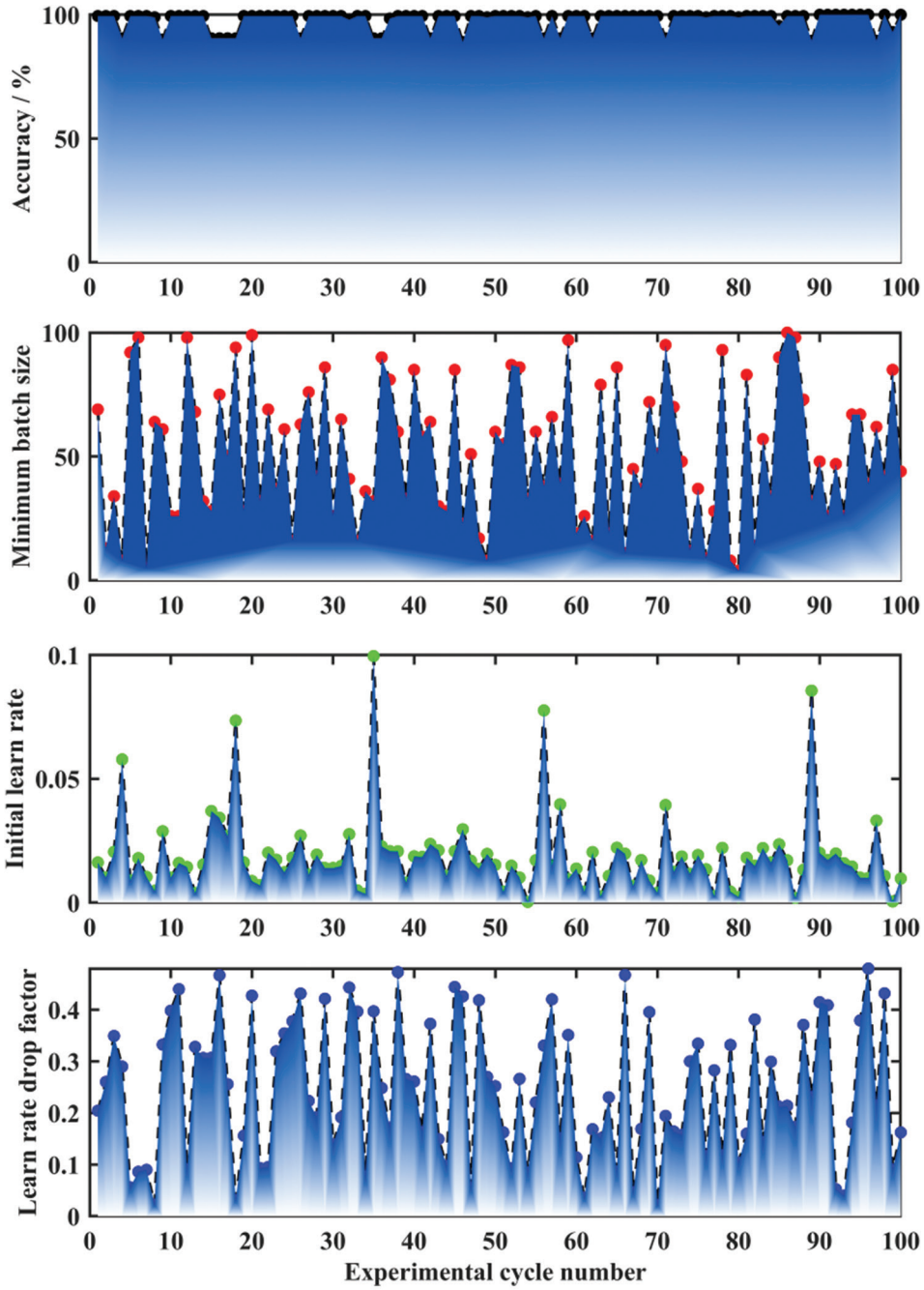

Figure 5. Accuracy and network optimal hyperparameter results for 100 rounds of NSGAIII optimized 1D-CNN models
Abbreviations: 1D-CNN: One-dimensional convolutional neural network; NSGAIII: Non-dominated sorting genetic algorithm III

average value, indicating that the model lacks the ability to regress non-linear high-dimensional data.

(ii) From the perspective of STD performance, both the BPNN model and the RBF model have significant recognition instability characteristics. The STD value of the BPNN accuracy index reached 22.6859%, whereas the STD values (RMSE and R-square) of the RBF model were 4.8144 and 914.9548, respectively. On the contrary, the STD values of multiple indicators of other network models were relatively small. The GRNN model performed best, with accuracy, MAE, RMSE, and R-square being 1.9778%, 0.0112, 0.0226, and 0.0099, respectively.

Figure 7 is a box plot of 100 rounds of earthquake and

Table 7. Statistical table of calculated results of multi-round seismic and blasting classification with different network training functions

Training function	Mean					STD				
	Accuracy (%)	MAE	MBE	R-square	RMSE	Accuracy (%)	MAE	MBE	R-square	RMSE
SGD-M	97.2500	0.0859	0.0114	0.6834	0.1408	3.9984	0.0627	0.0165	0.3909	0.0882
RMSrop	97.8750	0.0714	-0.0027	0.8386	0.1307	2.5229	0.0239	0.0289	0.0769	0.0243
Adam	99.5000	0.0620	0.0010	0.8848	0.1056	1.1391e-16	0.0109	0.0105	0.0272	0.0118

Abbreviations: Adam: Adaptive moment estimation; MAE: Mean absolute error; MBE: Mean squared error; RMSE: Root mean squared error; RMSrop: Root mean square propagation; R2: R-squared; SGD-M: Stochastic gradient descent with momentum.

Table 8. Comparison of 100 rounds of earthquake and blasting prediction statistics for multiple neural network models

Prediction model	Mean				STD			
	Accuracy (%)	MAE	RMSE	R^2	Accuracy (%)	MAE	RMSE	R^2
GRNN	88.150088	0.1925	0.3034	0.114	1.9778	0.0112	0.0226	0.0099
BPNN	40.4450	0.6719	0.7650	−5.433	22.6859	0.2593	0.2536	4.8606
RBF	81.0450	1.3234	5.7528	−528.6682	4.0961	0.9936	4.8144	914.9548
PNN	11.8500	0.8815	0.9388	−7.6719	1.9778	0.0198	0.0106	1.4469
1D-CNN	89.8200	0.2022	0.3005	0.1940	5.8108	0.0811	0.0986	0.4354
NSGAIII1D-CNN	97.8200	0.0795	0.1302	0.7361	3.5338	0.0558	0.0777	0.3366

Abbreviations: 1D-CNN: One-dimensional convolutional neural network; BPNN: Back propagation neural network; GRNN: Generalized regression neural network; MAE: Mean absolute error; NSGAIII: Non-dominated sorting genetic algorithm III; PNN: Probabilistic neural network; RBF: Radial basis function neural network; RMSE: Root mean squared error; R2: R-square.

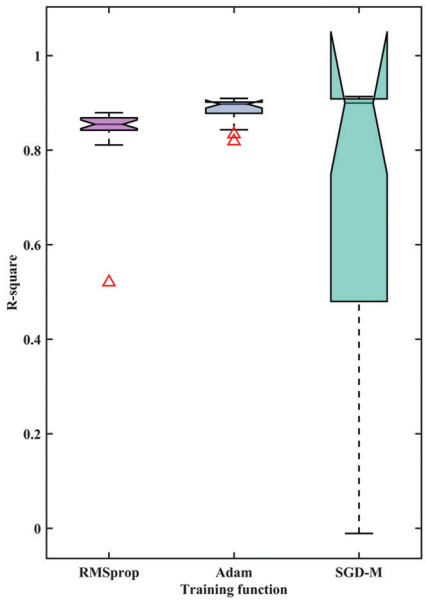

Figure 6. Box plot of predicted R-squared results of the multi-round NSGAIII-1D-CNN model with different training functions
Abbreviations: 1D-CNN: One-dimensional convolutional neural network; Adam: Adaptive moment estimation; NSGAIII: Non-dominated sorting genetic algorithm III; RMSrop: Root mean square propagation; SGD-M: Stochastic gradient descent with momentum

blasting signal recognition results under different neural network models, which can be used to simultaneously reflect the data discreteness and mathematical statistical information of multiple groups of earthquake and blasting classification results. The upper and lower boundary line indicators of the box in the figure represent the upper quartile (Q3) and lower quartile (Q1) of the positioning results, respectively. The solid line in the box represents the median of the positioning result. The "+" marked data is judged as an abnormal point by the box plot, and the horizontal solid lines distributed above and below the box represent the maximum and minimum values, respectively.

Figure 7A reveals the accuracy statistics of 100 rounds of earthquake and blast recognition for six neural network models. The medians of the box plots of the models GRNN, RBF, 1D-CNN, and NSGAIII-1D-CNN are relatively high, all above 80%. The recognition accuracy of the PNN model is relatively poor, and its box-plot interquartile range (IQR, *i.e.*, the difference between Q1 and Q3) value, median, upper quartile, and lower quartile are all below 20%, which is not good at processing high-dimensional and non-linear data sets. The recognition results of the BPNN model are highly random, with a difference of more than 80 percentage points between its maximum and minimum values, and an IQR value close to 40%.

Figure 7B reveals the MAE results of 100 rounds of earthquake and explosion recognition for the six neural

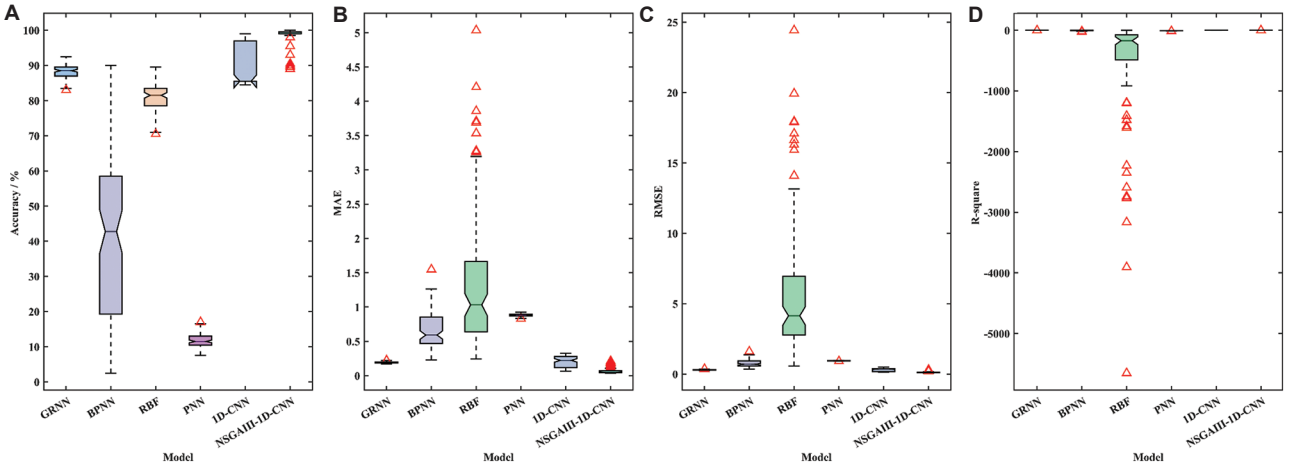

Figure 7. (A-D) Box plot of the prediction results of NSGAIII-1D-CNN compared with other neural network models under 100 rounds of recognition experiments
Abbreviations: 1D-CNN: One-dimensional convolutional neural network; NSGAIII: Non-dominated sorting genetic algorithm III

network models. The median, lower quartile, and upper quartile of the MAE set of the models GRNN, 1D-CNN, and NSGAIII-1D-CNN are all low – all below 0.3 – and there are no large outliers and extreme values; while the recognition performance of the RBF and BPNN models is extremely unstable, with many outliers with MAE exceeding 1.5, and the median and upper quartile both exceeding 0.5; in addition, although the PNN model shows strong recognition stability, and multiple index values are very close – it is far inferior to the NSGAIII-1D-CNN and other models in terms of prediction error.

Figure 7C reveals the RMSE results of 100 rounds of earthquake and explosion identification of six neural network models. The overall performance of the models GRNN, BPNN, 1D-CNN, PNN and NSGAIII-1D-CNN are relatively consistent, and most indicators are <1, proving that most of the predicted regression values of these network models are close to the theoretical label values; however, the RBF model shows significant regression anomalies, with a large number of outliers and large RMSE values. Its narrow and long box also shows that the model has the characteristics of poor stability.

Figure 7D reveals the R-squared results of 100 rounds of earthquake and blast identification for the six neural network models. The overall performance of the models GRNN, BPNN, 1D-CNN, PNN, and NSGAIII-1D-CNN is relatively consistent, and the R-square index is distributed very slightly around zero. However, the RBF model has poor regression interpretation ability for the CEEMDAN-MPE feature set, and its box plot shows a large number of outliers and unusual R-squared minima, which basically indicates that the model does not have good non-linear and non-stationary data processing capabilities.

4.4. Analysis of influencing factors of NSGAIII-1D-CNN model

4.4.1. Neural network training function

The neural network training function, also known as the learning function, is a key computing module in the neural network classification prediction model. It has a certain degree of influence on the accuracy of the precise distinction between earthquakes and explosions and the stability of the model. Common deep learning network training functions include:

(i) SGD-M: The traditional stochastic gradient descent method will oscillate on the steepest descent path. The introduction of momentum can accelerate convergence and suppress oscillation behavior; to minimize the loss function $E(\theta_t)$, the solver makes the iteration move in the negative gradient direction of the loss and updates the weights and biases of the network parameter vector θ in real time, that is, $\theta_{t+1} = \theta_t - \alpha \nabla E\theta_t + \gamma(\theta_t - \theta_{t-1})$, where α and γ are the learning rate and momentum values.

(ii) Root mean square propagation (RMSrop): It performs exponential weighted averaging of the square of the gradient and uses a dynamic learning rate and dynamic loss function that match the gradient size to improve the problem of oscillation convergence of the previous gradient descent method on complex surfaces. It only stores the exponential value of the square of the gradient and is suitable for fast processing of non-stationary targets such as audio.

(iii) Adaptive moment estimation (Adam): It combines the advantages of momentum and RMSrop. It can balance the first-order and second-order moments of the gradient by adaptively adjusting the learning

rate, eliminating oscillations in the update process, converging quickly, and being insensitive to the learning rate. It is suitable for processing large-scale problems such as NLP and time series modeling.

4.4.2. Comparison of prediction effects of NSGAIII-1D-CNN model under different training functions

The experiment in this section is designed as a 20-round cyclic classification experiment. The model is still the NSGAIII-1D-CNN model proposed in this paper. The training set used is fixed to the CEEMDAN-MFE sample set of 1000×11. The parameters of the NSGAIII model, such as population size, maximum number of iterations, crossover percentage, mutation percentage, and mutation rate, are set to 30, 10, 0.5, 0.5, and 0.02, respectively. The parameters of the 1D-CNN model, such as Max Epochs and Learn Rate Drop Period, are set to 50 and 20, respectively. The experimental results are shown in Table 7 and Figure 6.

Table 7 is a statistical table of the calculation results of multiple rounds of earthquake and blasting classification under different network training functions (Net Training Function). It uses the expected mean (Mean) and STD to statistically analyze the error trend and regression effect of multiple rounds of classification results. The specific indicators are accuracy (%), MAE, MBE, R-square, and RMSE. It can be seen from Table 7 that:

(i) From the performance of the STD indicator, the NSGAIII-1D-CNN model using Adam as the training function has stronger classification stability and consistency of prediction results. The STD of its accuracy (%), MAE, MBE, R-square, and RMSE are 1.1391e-16, 0.0109, 0.0105, 0.0272, and 0.0118, respectively; the classification result consistency of the NSGAIII-1D-CNN model with RMSrop as the training function is slightly better than the statistical results of the model using the SGD-M function. The only difference is that the STD value of the MBE indicator is slightly larger. However, considering that the positive and negative deviations of the MBE indicator may offset each other, it is not as accurate as the MAE indicator in reflecting the degree of network prediction error. The performance of the MBE indicator can be ignored here.

(ii) From the perspective of expected mean (Mean), the average prediction accuracy of the NSGAIII-1D-CNN model of the three network training functions is ranked as follows: Adam > SGD-M > RMSrop, among which the performance of each indicator of SGD-M and RMSrop is not much different, that is, the mean deviations of accuracy, MAE, MBE, R-square, and RMSE are 0.625%, 0.0145, 0.0141, 0.1552, and 0.0101, respectively. It is worth noting that the MBE of the RMSrop training function is negative, indicating that the model has a negative bias and underestimation trend.

Figures 6,8-11 are box-plots of the prediction results of multiple rounds of NSGAIII-1D-CNN models under different training functions, which can be used to simultaneously reflect the data discreteness and mathematical statistical information of multiple groups of earthquake and blasting classification results. The upper and lower boundary line indicators of the box in the figure represent the upper quartile (Q3) and lower quartile (Q1) of the positioning results, respectively. The solid line in the box represents the median of the positioning results. The "+" marked data is judged as an abnormal point by the box plot. The horizontal solid lines distributed above and below the box represent the maximum and minimum values, respectively.

Figure 8 reveals the prediction accuracy results of 20 rounds of NSGAIII-1D-CNN model for three training functions. Among them, the classification performance of earthquake and explosion of the training function "Adam" is relatively good, without obvious outliers and calculation divergence; the classification result of the training function "RMSprop" has one outlier, and its accuracy value is below 88%, which is almost 10 percentage points lower than the classification average of 97.8750%, indicating that there is a large room for improvement in the stability of its model;

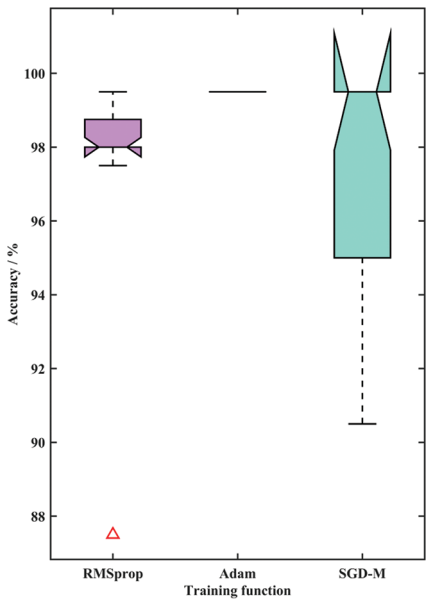

Figure 8. Box plot of prediction accuracy results of the multi-round NSGAIII-1D-CNN model with different training functions
Abbreviations: 1D-CNN: One-dimensional convolutional neural network; NSGAIII: Non-dominated sorting genetic algorithm III

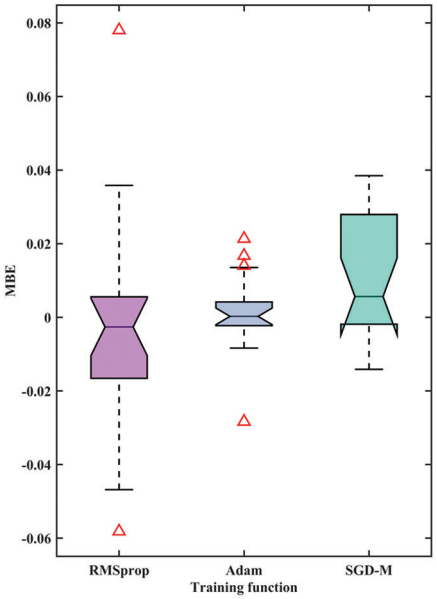

Figure 9. Box plot of predicted MBE results of the multi-round NSGAIII-1D-CNN model with different training functions
Abbreviations: 1D-CNN: One-dimensional convolutional neural network; Adam: Adaptive moment estimation; MBE: Mean squared error; NSGAIII: Non-dominated sorting genetic algorithm III; RMSrop: Root mean square propagation; SGD-M: Stochastic gradient descent with momentum

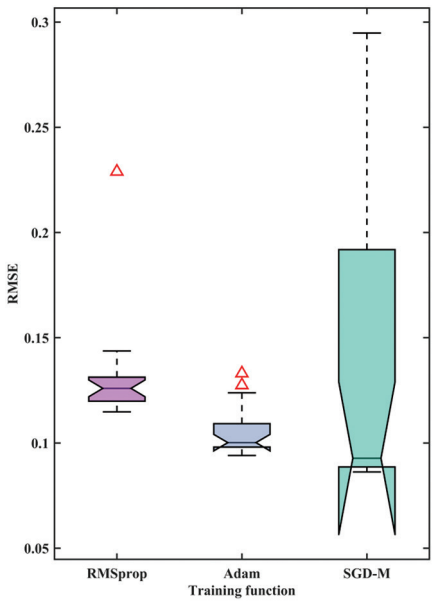

Figure 10. Box plot of predicted RMSE results of multi-round NSGAIII–1D-CNN model with different training functions
Abbreviations: 1D-CNN: One-dimensional convolutional neural network; Adam: Adaptive moment estimation; NSGAIII: Non-dominated sorting genetic algorithm III; RMSE: Root mean squared error; RMSrop: Root mean square propagation; SGD-M: Stochastic gradient descent with momentum

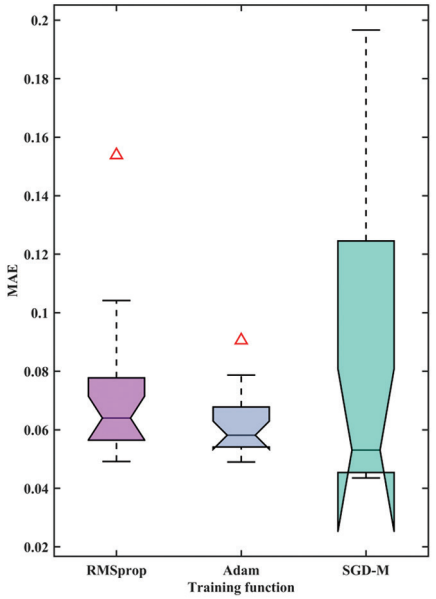

Figure 11. Box plot of predicted MAE results of the multi-round NSGAIII-1D-CNN model with different training functions
Abbreviations: 1D-CNN: One-dimensional convolutional neural network; Adam: Adaptive moment estimation; MAE: Mean absolute error; NSGAIII: Non-dominated sorting genetic algorithm III; RMSrop: Root mean square propagation; SGD-M: Stochastic gradient descent with

the classification result of the training function "SGD-M" has no outliers, but its IQR exceeds 4%, and its minimum value is very close to 90%, indicating that there is still room for improvement to a certain extent.

Figure 9 reveals the MBE results predicted by the NSGAIII-1D-CNN model for 20 rounds of three training functions. The classification results of the training function "Adam" tend to be biased and balanced, with the median of its box plot close to 0 and the IQR value within 0.01, indicating that the model has no significant positive or negative error bias. The classification results of the training function "RMSprop" have two MBE outliers, and the IQR value exceeds 0.02, showing a certain degree of negative bias. The IQR value of the box plot of the training function "SGD-M" reaches 0.03, and the position of the median shows that the model prediction shows an obvious positive bias.

Figure 6 reveals the R-square results predicted by the NSGAIII-1D-CNN model for 20 rounds of three training functions. The median and IQR values in the box plots of the training function "Adam" and the training function "RMSprop" are slightly different, and both the median and mean are greater than 0.8, indicating that both have strong model regression explanatory power in terms of the R-squared indicator. The IQR value of the box plot

of the training function "SGD-M" exceeds 0.4, and the minimum value is close to 0, reflecting that the calculation performance of this function is highly unstable.

Figure 10 reveals the RMSE results of 20 rounds of NSGAIII-1D-CNN model predictions for three training functions. The RMSE values of the prediction results of the training functions "Adam" and "RMSprop" both showed abnormal outliers, and the IQR value and the median of the box plot of the former were slightly smaller than those of the latter. The IQR value of the box plot of the training function "SGD-M" exceeded 0.1, and the maximum RMSE tended to 0.3, revealing that the prediction results of the NSGAIII-1D-CNN model using this function as the training function generally had large errors and unstable performance.

Figure 11 reveals the MAE results of 20 rounds of NSGAIII-1D-CNN model predictions for three training functions. The median MAE of the multi-round prediction results of the training function "Adam" tends to 0.06, its IQR value is also less than 0.02, and the only outlier is also less than 0.1, which proves that the training function can better minimize the deviation between the network prediction value and the theoretical value; the classification result of the training function "RMSprop" has a slightly larger MAE outlier, and its IQR value and the median of the box plot are slightly larger than "Adam"; the IQR value and maximum value of the box plot of the training function "SGD-M" are close to 0.08 and 0.2, respectively. Although the median is slightly smaller than that of the other two training functions, it is not enough to make up for the defect of the large prediction error of this training function.

5. Discussion

This study achieved an average recognition accuracy of 97.82% on 1000 sets of measured data (883 earthquakes and 117 explosions) through the innovative combination of CEEMDAN-MFE and NSGAIII-1D-CNN. This achievement is mainly due to three key technical breakthroughs:

CEEMDAN decomposition uses an optimized parameter combination of noise STD 0.2 and 24 noise additions, combined with a dynamically decreasing noise coefficient, to effectively solve the modal aliasing problem of traditional EMD. This method successfully decomposes earthquake and explosion signals into 11 IMF components with clear physical meanings, laying a solid foundation for subsequent feature extraction.

MFE feature extraction selects the optimal parameter combination of $m = 2$, $r = 0.2$, and $n = 2$, and constructs a highly discriminative feature matrix by calculating the entropy values of the first 8 IMF components (excluding the last three low-frequency noise-dominated components). The data in Table 2 shows that this feature set makes the NSGAIII-1D-CNN model have an MAE as low as 0.0795 and an R^2 of 0.7361 in 100 rounds of random experiments, which is significantly better than the comparison model.

The NSGAIII optimization stage sets the population size to 50 and the maximum iteration to 50 generations, and optimizes the hyperparameters of 1D-CNN through dual objectives (minimizing MBE and maximizing R^2). This strategy enables the model to control the RMSE to 0.1302 whereas maintaining an average accuracy of 97.82%. When the Adam optimizer is used, the peak performance of the model can reach 99.5%, which has obvious advantages over SGD-M and RMSprop.

The end-to-end delay of the current model for completing a single recognition on standard hardware (Intel i7) is 200 ms, of which CEEMDAN-MFE feature extraction accounts for 60%. Through technologies such as model quantization, the memory usage has been compressed to 8.7 MB, meeting the deployment requirements of edge devices. In terms of practical applications, the current system has two main limitations: first, the recognition accuracy of signals with a signal-to-noise ratio below 5 dB will drop by about 15%, which is mainly due to the interference of noise on the MFE calculation; second, although the window of 4000 sampling points can maintain feature integrity during real-time processing, it increases the delay by about 200 ms. However, the system still maintains an accuracy rate of more than 90% in tests in different regions such as Qinghai and Sichuan, proving that it has strong environmental adaptability.

The comparison with existing technologies highlights the value of this study: compared with traditional 1D-CNN (89.82% accuracy) and GRNN (88.15%), the accuracy of this model is improved by 8–10 percentage points; in terms of regression indicators, MAE (0.0795) is reduced by more than 60% compared with the comparison model. These improvements are reflected in more reliable recognition performance in actual monitoring, such as successfully distinguishing 97.3% of blasting interference events in the 2023 Luding aftershock sequence.

Future research will be deepened in three directions: first, develop a dynamic adjustment mechanism for CEEMDAN parameters with adaptive signal-to-noise ratio to improve stability under extremely low signal-to-noise ratio; second, deploy a chip-level online learning system to achieve continuous optimization of model parameters; third, integrate multimodal data of geological environment to build a more interpretable intelligent discrimination

system. These improvements will further enhance the applicability and reliability of this technology in actual earthquake monitoring scenarios.

6. Conclusion

This study proposes a hybrid prediction model that integrates CEEMDAN-MFE feature extraction and NSGAIII-optimized 1D-CNN. Through theoretical innovation and technological breakthroughs, the recognition accuracy and model stability of earthquake and explosion events are significantly improved. Experimental verification based on 1000 measured signals shows that the proposed CEEMDAN-MFE feature extraction method can effectively capture the essential differences in the non-linear dynamic characteristics of earthquake and explosion signals, and the constructed feature matrix significantly enhances the pattern separability of the signal. The 1D-CNN model optimized by NSGAIII multi-objective achieved an average accuracy of 97.82% in 100 rounds of random experiments. All performance indicators were significantly better than those of the traditional neural network model, verifying the synergistic advantages of the network structure and automatic optimization of hyperparameters. Despite the remarkable research results, this study still has limitations such as limited data coverage, the need to improve the accuracy of microseismic signal recognition, and the need to optimize edge computing efficiency. Based on the current research foundation, future work will focus on in-depth research on cross-regional generalization verification, model lightweight design, and multimodal data fusion. By constructing a larger-scale multi-tectonic belt data set, developing a compression algorithm based on knowledge distillation, and integrating waveform data with geological environment parameters, the practicality and generalization ability of the model will be further improved. This study not only provides a new technical solution for the field of earthquake monitoring, but its innovative research methodology also provides a useful reference for other time-varying signal processing fields, which has important theoretical value and practical significance.

Acknowledgments

None.

Funding

This research was financially supported by Mahasarakham University; Open Fund of Wuhan Gravitation and Solid Earth Tides, National Observation and Research Station, (No.WHYWZ202406, WHYWZ202208); Scientific Research Fund of Institute of Seismology, China Earthquake Administration and National Institute of Natural Hazards, MEM, (No. IS202236328, IS202436357); The Spark Program of Earthquake Technology of CEA, (No. XH24025YC); Earthquake Monitoring and Forecasting and Early Warning Tasks for 2025, (No. CEA-JCYJ-202502015); Chengdu Jincheng College Green Data Integration Intelligence Research and Innovation Project (No. 2025-2027); and the High-Quality Development Research Center Project in the Tuojiang River Basin (No. TJGZL2024-07).

Conflicts of interest

The authors declare they have no competing interests.

Author contributions

Conceptualization: Cong Pang, Tianwen Zhao, Pornntiwa Pawara

Formal analysis: Cong Pang, Guoqing Chen, Piyapatr Busababodhin, Pornntiwa Pawara

Investigation: Piyapatr Busababodhin, Chawei Li, Zhongya Li, Pornntiwa Pawara

Methodology: Cong Pang, Tianwen Zhao, Guoqing Chen, Chawei Li, Zhongya Li

Writing–original draft: Cong Pang, Tianwen Zhao, Guoqing Chen, Pornntiwa Pawara

Writing–review & editing: Cong Pang, Tianwen Zhao, Guoqing Chen, Pornntiwa Pawara

Availability of data

This study integrates 1000 sets of strong earthquake observation data and explosion data from various regions in and around China, mainly from earthquake case data publicly shared by the National Earthquake Data Center (NEDC, data.earthquake.cn), the Institute of Engineering Mechanics of the China Earthquake Administration (IEM, CEA) and China Institute of Water Resources and Hydropower Research (CIWHR).

References

1. Johnson JA, Mutchnick AB. Identification of wall tension fractures caused by earthquakes, blasting, and pile driving. *Environ Eng Geosci*. 2016;22(2):131-139.

   doi: 10.2113/gseegeosci.22.2.131

2. Dong LJ, Wesseloo J, Potvin Y. Discriminant models of blasts and seismic events in mine seismology. *Int J Rock Mech Min Sci*. 2016;86:282-291.

   doi: 10.1016/j.ijrmms.2016.04.021

3. Lythgoe K, Loasby A, Hidayat D, Wei S. Seismic event detection in urban Singapore using a nodal array and frequency domain array detector: Earthquakes, blasts, and thunder quakes. *Geophys J Int*. 2021;226(3):1542-1557.

doi: 10.1093/gji/ggab135

4. Saad M, Soliman MS, Chen Y, Amin AA, Abdelhafiez HE. Discriminating earthquakes from quarry blasts using capsule neural network. *IEEE Geosci Remote Sens Lett*. 2022;19:1-5.

   doi: 10.1109/LGRS.2022.3207238

5. Wang S, Hu Y, Chen H, Chen X. An energy-concentrated transform for improved time-frequency representation of seismic signals. *IEEE Signal Process Lett*. 2025;32:2084-2088.

   doi: 10.1109/LSP.2025.3565164

6. Rivera E, Ruiz S, Madariaga R. Spectrum of strong-motion records for large magnitude Chilean earthquakes. *Geophys J Int*. 2021;226(2):1045-1057.

   doi: 10.1093/gji/ggab128

7. Mei W, Li M, Pan PZ, Pan J, Liu K. Blasting induced dynamic response analysis in a rock tunnel based on combined inversion of Laplace transform with elasto-plastic cellular automaton. *Geophys J Int*. 2020;225(1):699-710.

   doi: 10.1093/gji/ggaa615

8. Matsushima M, Honkura Y, Kuriki M, Ogawa Y. Circularly polarized electric fields associated with seismic waves generated by blasting. *Geophys J Int*. 2013;194(1):200-211.

   doi: 10.1093/gji/ggt110

9. Xiao Y, Guo J, Chen S, Liu L, Chen B. Digitalization of rock fracture signal identification from tunnel microseismic data. *IEEE Geosci Remote Sens Lett*. 2024;21:1-5.

   doi: 10.1109/LGRS.2024.3399271

10. Zhou J, Ba J, Castagna JP, Guo Q, Yu C, Jiang R. Application of an STFT-based seismic even and odd decomposition method for thin-layer property estimation. *IEEE Geosci Remote Sens Lett*. 2019;16(9):1348-1352.

    doi: 10.1109/LGRS.2019.2901261

11. Geetha K, Hota MK. Seismic random noise attenuation using optimal empirical wavelet transform with a new wavelet thresholding technique. *IEEE Sens J*. 2024;24(1):596-606.

    doi: 10.1109/JSEN.2023.3334819

12. Alvanitopoulos PF, Papavasileiou M, Andreadis I, Elenas A. Seismic intensity feature construction based on the Hilbert-Huang transform. *IEEE Trans Instrum Meas*. 2012;61(2):326-337.

    doi: 10.1109/tim.2011.2161934

13. Chen CH, Wang CH, Liu JY, Liu C, Liang WT, Yen HY. Identification of earthquake signals from groundwater level records using the HHT method. *Geophys J Int*. 2010;180(3):1231-1241.

    doi: 10.1111/j.1365-246X.2009.04473.x

14. Küperkoch L, Meier T, Lee J, Friederich W. Automated determination of P-phase arrival times at regional and local distances using higher order statistics. *Geophys J Int*. 2010;181(2):1159-1170.

    doi: 10.1111/j.1365-246X.2010.04570.x

15. Zhu J, Zhou Y, Liu H, *et al*. Rapid earthquake magnitude classification using single station data based on machine learning. *IEEE Geosci Remote Sens Lett*. 2024;21:1-5.

    doi: 10.1109/lgrs.2023.3346655

16. Samal P, Hashmi MF. Ensemble median empirical mode decomposition for emotion recognition using EEG signal. *IEEE Sens Lett*. 2023;7(5):1-4.

    doi: 10.1109/lsens.2023.3265682

17. Chen J, Heincke B, Jegen M, Moorkamp M. Using empirical mode decomposition to process marine magnetotelluric data. *Geophys J Int*. 2012;190(1):293-309.

    doi: 10.1111/j.1365-246X.2012.05470.x

18. Li B, Huang H, Wang T, Wang M, Wang P. Research on Seismic Signal Classification and Recognition Based on EEMD and CNN. Presented at: *2020 IEEE 3rd International Conference on Electronics and Communication Engineering (ICECE)*. Shenzhen, China; 2020. p. 83-88.

    doi: 10.1109/ICECE51594.2020.9353037

19. Zhang D, Wang Y, Zhu T, Ma GW. Mode identification method of long span steel bridge based on CEEMDAN and SSI algorithm. *Earthquake Eng Resil*. 2024;3(3):388.

    doi: 10.1002/eer2.89

20. Wu S, Guo H, Zhang X, Wang F. Short-term photovoltaic power prediction based on CEEMDAN and hybrid neural networks. *IEEE J Photovolt*. 2024;14(6):960-969.

    doi: 10.1109/jphotov.2024.3453651

21. Wang J, Dai B, Zhang T, Qi L. A novel hybrid model of CEEMDAN-CNN-SAGU for Shanghai copper price prediction. *IEEE Access*. 2024;12:25176-25187.

    doi: 10.1109/access.2024.3365558

22. Tian S, Bian X, Tang Z, Yang K, Li L. Fault diagnosis of gas pressure regulators based on CEEMDAN and feature clustering. *IEEE Access*. 2019;7:132492-132502.

    doi: 10.1109/ACCESS.2019.2941497

23. Li J, Yao R. Field deployment of natural gas pipeline pre-warning system with CEEMDAN denoising method. *IEEE Photon J*. 2024;16(4):1-8.

    doi: 10.1109/JPHOT.2024.3421275

24. Pan L, Liu M, Chen R, Ma S. Research on Seismic Signal Identification and Magnitude Prediction Model Based on Sample Entropy and Machine Learning. Presented at: 2024 *IEEE 2nd International Conference on Sensors, Electronics and Computer Engineering (ICSECE)*. Beijing, China; 2024. p. 1586-1592.

    doi: 10.1109/icsece61636.2024.10729556

25. Aggarwal M. Bridging the gap between probabilistic and fuzzy entropy. *IEEE Trans Fuzzy Syst*. 2020;28(9):2175-2184.

doi: 10.1109/TFUZZ.2019.2931232

26. Ali M, Nathwani K. Exploiting wavelet scattering transform and 1D-CNN for unmanned aerial vehicle detection. *IEEE Signal Process Lett*. 2024;31:1790-1794.

doi: 10.1109/LSP.2024.3421961

27. Kail R, Burnaev E, Zaytsev A. Recurrent convolutional neural networks help to predict location of earthquakes. *IEEE Geosci Remote Sens Lett*. 2022;19:1-5.

doi: 10.1109/lgrs.2021.3107998

28. Sivanjaneyulu Y, Manikandan MS, Boppu S, Cenkeramaddi LR. Resource-efficient derivative PPG-based signal quality assessment using one-dimensional CNN with optimal hyperparameters for quality-aware PPG analysis. *IEEE Access*. 2024;12:141251-141267.

doi: 10.1109/access.2024.3464231

29. Perera S, Witharana C, Manos E, Liljedahl AK. Hyperparameter optimization for large-scale remote sensing image analysis tasks: A case study based on permafrost landform detection using deep learning. *IEEE Access*. 2024;12:43062-43077.

doi: 10.1109/ACCESS.2024.3379142

30. Wang Y, Wang Y, Jiang K, Zheng W, Song M. Adaptive grid search-based pulse phase and Doppler frequency estimation for XNAV. *IEEE Trans Aerosp Electron Syst*. 2024;60(3):3707-3717.

doi: 10.1109/TAES.2024.3361431

31. Ren L, Li Y, Zhou S. An improved NSGA-III algorithm for scheduling ships arrival and departure at the main channel of Tianjin Port. *IEEE Access*. 2024;12:131442-131457.

doi: 10.1109/access.2024.3457526

32. Srinivas N, Deb K. Muiltiobjective optimization using nondominated sorting in genetic algorithms. *Evol Comput.* 1994;2(3):221-248.

doi: 10.1162/evco.1994.2.3.221

33. Deb K, Pratap A, Agarwal S, Meyarivan TAMT. A fast and elitist multiobjective genetic algorithm: NSGA-II. *IEEE Trans Evol Comput.* 2002;6(2):182-197.

doi: 10.1109/4235.996017

34. Deb K, Jain H. An evolutionary many-objective optimization algorithm using reference-point-based nondominated sorting approach, part I: solving problems with box constraints. *IEEE Trans Evol Comput*. 2013;18(4):577-601.

doi: 10.1109/TEVC.2013.2281535